



[www.sciencemag.org/cgi/content/full/333/6048/1421/DC1](http://www.sciencemag.org/cgi/content/full/333/6048/1421/DC1)

Supporting Online Material for

***Australopithecus sediba* at 1.977 Ma and Implications for the Origins of the Genus *Homo***

Robyn Pickering,\* Paul H. G. M. Dirks, Zubair Jinnah, Darryl J. de Ruiter, Steven E. Churchil, Andy I. R. Herries, Jon D. Woodhead, John C. Hellstrom, Lee R. Berger

\*To whom correspondence should be addressed. E-mail: [r.pickering@unimelb.edu.au](mailto:r.pickering@unimelb.edu.au)

Published 9 September 2011, *Science* **333**, 1421 (2010)  
DOI: 10.1126/science.1203697

**This PDF file includes:**

SOM Text S1 to S4

Figs. S1 to S8

Tables S1 to S3

References (23–73)

Supporting Online Material for

***Australopithecus sediba* at 1.977 Ma and implications for the origins of  
the genus *Homo***

Robyn Pickering\*, Paul H.G.M. Dirks, Zubair Jinnah, Darryl J. de Ruiter, Steven E.  
Churchill, Andy I.R. Herries, Jon D. Woodhead, John C. Hellstrom, Lee R. Berger

\*To whom correspondence should be addressed. Email: [r.pickering@unimelb.edu.au](mailto:r.pickering@unimelb.edu.au)

SOM Text S1 to S4

Figs. S1 to S8

Tables S1 to S3

References (23-27)

## **TEXT S1. Fossil specimens considered to belong to *Homo* dating to older than 2.0 Ma**

The following specimens have been assigned to the genus *Homo*, and all of them are reported to be older than 2.0 Ma. In this text we discuss the evidence pertaining to provenience and taxonomic affiliation.

### **SOUTH AFRICA**

A number of fossils from Sterkfontein Member 4 and 5 have been classified as *Homo* or have been suggested to show affinities with *Homo*. The debate surrounding what comprises Member 5 and associated deposits at Sterkfontein continues (2, 14, 23). Among these associated deposits is Member 5a (aka Stw 53 infill) which has been referred to as a later phase of Member 4 with an original age estimate of greater than 2.0 Ma (23). More recent work suggests that this deposit, along with Member 5 is less than 1.8 Ma based on a combination of fauna, ESR, U-Pb and palaeomagnetism (2,14). Given that the Member 5 deposits themselves have been largely removed by excavation, the original provenience of these fossils is somewhat uncertain given the long term excavation of the site and the fact that the stratigraphic views of what belongs to Member 4 and 5 have changed over time. However, as they have been referred to *Homo*, we discuss these fossils below.

**Sts 19.** Since its discovery in 1947, Sts 19 has been commonly referred to *Au. africanus*. However, the possibility has been raised that Sts 19 might represent early *Homo* (24), though this hypothesis has been challenged (25). Although the taxonomic status of Sts 19 is deemed uncertain by some (26), we do not consider the evidence linking it to early *Homo* to be sufficiently compelling to warrant inclusion in the genus. This is based on the fact that many of the basicranial features thought to link Sts 19 with *Homo* are also evident in other australopith specimens, and thus are not exclusive to *Homo* (25). In addition, the actual provenience of Sts 19 within the Sterkfontein Formation is not certain, thus it is not clear if it actually predates 2.0 Ma, or if it possibly derived from the younger sediments.

**Stw 53.** When it was first discovered in 1976, the Sterkfontein cranium Stw 53 was tentatively assigned to the genus *Homo*, with a possible specific affiliation with *H. habilis* (27). Stw 53 came to be widely accepted as a representative of early *Homo* (28, 29, 30), eventually being firmly attributed to *H. habilis* (31). Stw 53 was originally reported to be from Member 5 of Sterkfontein, though it was later determined to be from a discrete deposit possibly representing a later phase of Member 4 (aka Member 5a), which has been dated to between 2.6 and 2.0 Ma (23, 32). This would potentially make it the oldest representative of early *Homo* in southern Africa. The assignment of Stw 53 to *Homo* has been challenged on both stratigraphic (32) and anatomical (2, 32) grounds, as the cranium shares numerous morphological characters with *Au. africanus*. Additionally, recent dating of the deposit using a combination of ESR, palaeomagnetism and U-Pb ages from the site suggest the deposit from which Stw 53 is likely derived dates to less than 1.8 Ma (1, 14). Most recently, Stw 53 has been designated as the type specimen of a new species, “*H. gautengensis*” (33), though given its close morphological similarities to *Au. africanus* (see especially refs 2, 32), there is little reason to consider it representative of a new species, in particular a species of *Homo*. These similarities with *Au.*

*africanus* include closely spaced temporal lines, marked post-orbital constriction, weakly developed supraorbital torus, narrow and non-projecting nasal bones, weakly developed but present anterior pillars, marked nasopalveolar prognathism, medial and lateral expansion of the frontal process of the zygomatic bone, and laterally flared zygomatics. In turn, minus its type specimen, there is little reason to consider “*H. gautengensis*” to be a valid taxon. The preponderance of anatomical evidence indicates that Stw 53 is best considered a (possibly later) form of *Au. africanus* that is not especially closely affiliated with early *Homo*, particularly considering the more derived, *Homo*-like appearance of MH1 of *Au. sediba*.

**Stw 151.** This specimen is comprised of a series of teeth and bone fragments that can be reconstructed into a relatively complete set of jaws and teeth of a juvenile individual aged about 5 years (34). Initially catalogued as being from “Member 4 or Member 5”, it appears that this specimen is derived from a separate deposit, originally estimated to be between 2.0-2.6 Ma (23), though in conjunction with Stw 53, this deposit might date to less than 1.8 Ma (1, 14). The most comprehensive analysis of this specimen raised the possibility that it is more derived toward *Homo* than the remainder of the Sterkfontein Member 4 *Au. africanus* sample (34), though the authors did not go so far as to attribute the specimen to the genus *Homo*. The main characters aligning Stw 151 with specimens attributed to early *Homo* reside in the BL reduction and MD elongation of the M<sub>1</sub>, the MD elongation of the M<sup>1</sup>, the differential development of the entoglenoid process relative to the temporal spine, and the more coronal orientation of the posterior surface of the petrous bone. Notwithstanding, the majority of cranial and dental characters align this specimen with *Au. africanus*, thus we agree that this specimen cannot yet be assigned to the genus *Homo*, while its age of greater than 2.0 Ma cannot be established with certainty, and is most likely less than 1.8 Ma (1, 14, 35).

**Additional isolated teeth from Sterkfontein Member 5.** These include the specimens SE 255, SE 1508, SE 1937, Stw 75, and Stw 80, all of which have been aligned with early *Homo*. However, we would stress that taxonomic allocation of isolated dental remains can be misleading. Most of these fossils have been associated with Member 5c (aka Member 5 West (1)), which has recently been suggested to date to less than 1.3 Ma (14). As a result, there is no indication of early *Homo* (i.e. *H. habilis* or *H. rudolfensis*) prior to 2.0 Ma in South Africa.

## **EAST AFRICA**

**KNM-BC1.** Originally discovered in 1965, the provenience of this temporal bone fragment was thought to be sound, and that, “there is little doubt that the fossil came from the Upper Fish Beds [site JM 85] and not from a higher horizon in the Chemeron Beds...” (36). The fossil was recovered as a surface find on what was referred to as “almost a bedding plane slope”, though an accompanying cross section of the discovery site indicates that the fossil came from a slope of approximately 26° at the edge of a stream. Some 25 years later the site was relocated and dated (37), and at 2.4 Ma suggested to be among the earliest evidence of *Homo* in the fossil record. The provenience of the specimen was considered affirmed by three sources: an undated, unpublished excavation report in the Bishop Archives of the National Museums of Kenya, a published paper originally presented at a conference, and a published catalogue of fossil hominids. However, neither of the latter two confirming sources

went beyond summarizing the evidence presented in the initial publication (36), thus they do not aid in establishing the provenience of the specimen (38).

Several characters were noted that linked KNM-BC1 to *Homo*, including a medially positioned mandibular fossa (possibly indicating cranial expansion), exposure of the tegmen tympani in the ceiling of the mandibular fossa, presence of an anteromedial recess, steep and restricted preglenoid plane, and a sagittally convex tympanic laterally (37, 39). However, the utility of these characters for phylogenetic interpretations is uncertain, as they all tend to vary across hominin taxa, and the specimen does not exhibit any unique affinity to specimens considered to belong to early *Homo* (10, 40, 41, 42). As a result, KNM-BC1 cannot be demonstrated to belong in the genus *Homo*, and in fact, has been postulated as a possible representative of the more recently named *Au. garhi* (43).

**UR 501.** This relatively complete mandible was recovered from the Plio-Pleistocene Chiwondo Beds in Malawi (44). It was recorded from stratigraphic Unit 3A in the Uraha Hill in the Chilumba area. The fossil was discovered in two halves some 20 cm apart, on the surface of a shallow slope (45). The joining surfaces between the two halves were covered by a calcareous matrix, suggesting that they were broken apart at some point in antiquity. The authors suggest that this breakage occurred prior to exposure on the surface. The left side is more weathered than the right, while the right was covered by calcareous matrix on its lingual side. The calcareous matrix on the right side also contained a ferric cementing agent that was used to source the mandible to the ferruginous calcimorphic paleosol of Unit 3A of the Uraha sedimentary sequence (46). However, the overlying sediment, Unit 3B, is also a ferruginous calcimorphic paleosol that the authors date to 2.0-1.5 Ma (44). As a result, there is a possibility that the UR 501 mandible is derived from higher in the sequence.

Even if we accept that UR 501 is derived from its claimed source, we would still dispute the age assigned to Unit 3A based on the fauna recovered from this layer. Several faunal lists have been presented for Unit 3A of the Chiwondo Beds (44, 47, 48), and where these faunal lists differ, we will rely on the most recent publication (48) for taxonomic determinations. Fossils assigned to Unit 3A were recovered from a series of northern and southern localities that the authors refer to as Karonga (north) and Uraha (south), though we will focus mainly on the Uraha region, as this is the source of the hominin in question. In the latest publication (48), Unit 3A is considered to fall within a broad time span bracketed by the latest appearance of *Nyanzachoerus jaegeri* at 3.75 Ma, and the latest appearance of *Notochoerus euilius* at 2.0. Detailed examination of the Uraha fauna reveals considerable admixture, casting additional doubt on the proposed age of 2.5 Ma for the mandible UR 501.

*Elephas recki atavus* is recorded at Uraha, a taxon dating to between 2.36-1.64 Ma elsewhere in East Africa (49). *Deinotherium* is also recognized at Uraha, though this genus exhibits a relatively long temporal span from ca. 5.0-1.6 Ma. *Hipparion* is recorded at Uraha, and was assigned an age of 2.9-2.3 Ma at the site based on the presence of robust ectostylids that are correlated with specimens from Members C and above in the Shungura sequence (47). However, Eisenmann (50) notes that an ectostylid is present in all *Hipparion* molars from Member C to Member G (2.85-1.9 Ma), and that there does not appear to be any change in ectostylid size over time (51). Eisenmann also discusses *Hipparion* fossils from the Koobi Fora sequence that correspond to the Shungura fossils, but which are derived from the Upper Burgi to the Okote Members (1.98-1.39 Ma). *Hippopotamus*, *Parapapio*, *Diceros bicornis*, and *Ceratotherium simum* are all found at Uraha, though since all of these genera appear

prior to 4.0 Ma, they are of no assistance here. The same could be said of *Giraffa pygmaea* and *G. stillei*, since although they are both extinct, both appear before 4.0 Ma, and both vanish less than 1.0 Ma. Since most of the bovids are identified to genus only, they do not aid in resolving the age of the deposit. *Metridiochoerus andrewsi* fossils are recorded at Uraha, and Bromage et al. (45) note that this taxon is reliably recorded from 2.95-1.74 elsewhere in East Africa. *Notochoerus euilus* fossils are known from Uraha, and date from ca. 3.75-2.0 Ma (52) in the African fossil record. A small number of teeth assigned to *Notochoerus scotti* are suggested to fall between 2.52-2.33 Ma based on their relatively short occlusal length and the small number of lateral pillar pairs (48). However, this taxon has a broader temporal span of ca. 2.8-1.8 Ma, thus this more constrained date is based on an arbitrary subdivision of the lineage, as White (52) indicates that this taxon changes little throughout its duration, thus we cannot be certain that the short occlusal length genuinely constrains the age of these fossils. The net effect is that there is no strong indication that the Uraha site or mandible should be dated at 2.5 Ma. Rather, there appear to be strong indications of admixture, thus the broad age reflected in the fauna from Unit 3A cannot be used to support the contention that UR 501 is 2.5 Ma. Combined with the possible uncertainty regarding the provenience of this surface discovery, the evidence supporting the existence of *Homo* prior to 2.0 Ma in Malawi is insufficient.

**Isolated teeth from Omo.** A collection of some 22 isolated molars, premolars, and a single canine, alongside a single fragmentary mandible, have been considered to show affinities to early *Homo* in Members E (2.4-2.36 Ma), F (2.36-2.33 Ma), and G (2.33-1.9 Ma) in the Omo Shungura sequence (53, 54). In the more comprehensive study, these teeth have been identified as “aff. *Homo* sp. indet.”, with their closest recognized similarity to *H. rudolfensis* (54). This study proceeded by separating “robust” from non-“robust” teeth, and then assessing the morphological affinities of these non-“robust” specimens. The more useful of the latter group were the P<sub>3</sub>s and M<sub>1</sub>s, though the resolving power of the diagnostic characters was limited. The P<sub>3</sub>s exhibited a *Homo*-like lack of asymmetry and strong development of the mesial marginal ridge; however, these are two characters out of a larger assemblage of eight characters that were determined to be uniquely derived toward *Homo* relative to *A. afarensis*, thus the linkage to *Homo* is not especially strong. The molars were less diagnostic, as only the M<sub>1</sub> could be linked to early *Homo*, and only in having a buccolingual breadth that is narrow relative to total crown area; in fact, three of the four relatively complete M<sub>1</sub>s referred to *Homo* displayed at least one character that aligned it with “robust” australopiths rather than *Homo*. The authors cautioned against drawing far reaching conclusions, as again the linkage to early *Homo* is not especially strong. As a result, the authors were notably cautious in their attribution of the specimens to *Homo*, thus their assignment to the category “aff. *Homo* sp. indet.” Attribution of isolated teeth to species is a difficult endeavor, thus these fossils from the Omo Shungura sequence are insufficient to document the existence of *Homo* prior to 2.0 Ma.

**KNM-WT 42718.** This isolated RM<sub>1</sub> was recovered in an apparently secure context via sieving operations in a newly recognized paleontological locality in the Lokalalei site complex, dated to ca. 2.34 Ma (55). The specimen was assigned to *Homo* based on both metrical and morphological features. In their metrical analysis it was noted that KNM-WT 42718 plotted outside the range of *Au. africanus*, but only if Sts 24, Stw 80, and Stw 151 were excluded from the *Au. africanus* sample. We agree that Stw

80 might possibly represent early *Homo*, though we disagree with the assertion that Sts 24 and Stw 151 also represent *Homo*. Stw 151 was reported to be a hominin more derived toward *Homo* than the rest of the *Au. africanus* sample, based in part on the BL narrow M<sup>1</sup> crown (34), though it was not assigned to *Homo* (see above). The M<sub>1</sub> of Sts 24 was suggested to be relatively BL narrow as seen in specimens of *H. habilis* (56), otherwise it conforms closely to the *Au. africanus* pattern from Sterkfontein (57). Given the morphological similarity of Sts 24 to the *Au. africanus* hypodigm, there is no reason to consider it as belonging to *Homo*, therefore there is no reason to exclude it from *Au. africanus* in metrical analyses. In addition, Prat et al. (55) included measures from a very restricted sample of hominins, in particular of *Au. africanus*, and an enlarged hypodigm including all *Au. africanus* M<sub>1</sub>s (excepting antimeres) reveals that KNM-WT 42718 plots within the range of this latter taxon.

Prat et al (55) reported a strong posterior probability value of  $p=0.8033$  that KNM-WT 42718 should be classified with early *Homo* via discriminant analysis. However, their restrictive australopith and early *Homo* samples excluded numerous specimens. When we re-compute posterior probabilities with comprehensive hominin samples of mandibular first molars, alongside large samples of gorillas ( $n=37$ ), chimpanzees ( $n=50$ ), and modern humans ( $n=43$ ), KNM-WT 42718 classifies with early *Homo* with a posterior probability of only  $p=0.5409$ . Substantial numbers of misclassifications are evident in the hominin samples, such that only 46.7% of the *Homo* specimens are correctly classified, while a total of only 60.2% of all hominins and apes are correctly classified.

Many of the characteristics that were listed as aligning KNM-WT 42718 with early *Homo* can be found in australopiths, even if not in the configuration seen in the Turkana tooth. Given the difficulty one encounters when attempting to taxonomically diagnose fragmented hominin remains, in particular isolated teeth, we not do consider the evidence in favor of early *Homo* prior to 2.0 Ma at West Turkana to be compelling.

**A. L. 666-1.** This fragmented maxilla was found in two main portions on the surface of a silt horizon in the previously unexplored Maka'amitalu Basin at Hadar in 1994 (58). An additional 30 fragments were recovered from the surface, and the entire specimen was reconstructed along a series of apparently fresh breaks. Excavation into the hillside revealed no additional hominin fragments, though several lithics and non-hominin bone fragments were recovered. The specimen was dated to ca. 2.33 Ma based on its position 80 cm below the Bouroukie Tuff 3 (BKT-3) of the Kada Hadar Member of the Hadar Formation. The stratigraphy of the area was later refined, and it was recognized that the maxilla is actually derived from the Busidima Formation (59), though this did not affect the dating of the BKT-3 marker tuff. The authors concluded that the specimen was eroded out of the siltstone that it was found lying on because the silt matrix filled the sinus cavities and tooth alveoli, a root cast commonly found in the silt horizon was located within a maxillary sinus, and the *in situ*, non-hominin bone fragments recovered during excavation showed identical preservation and patina to the maxilla.

Kimbel et al (13) cited 10 characters of the A.L. 666-1 maxilla that aligned it most closely with *Homo*. While the specimen does indeed align with fossils attributed to *Homo*, it does not do so to the exclusion of australopiths. In other words, several of the cited characters are equivocal as they are found in australopiths as well as *Homo*. In addition, some of the characters that align A.L. 666-1 with early *Homo* are not encountered in all specimens assigned to early *Homo*. Although A.L. 666-1 does

resemble *Homo* in some features, it is unclear whether these features are reliably and exclusively diagnostic of the genus. We do not presently know if these linking characters truly yield phylogenetic information (60). As a result, if some or all of the characters aligning A.L. 666-1 with *Homo* are not exclusively diagnostic of the genus, the identification of this specimen as *Homo* aff. *H. habilis* might not be conclusive. The *Au. sediba* fossils from Malapa highlight the need for caution when attributing isolated dentognathic remains to the species level, as fragmented remains can be extremely difficult to diagnose (2, 61). The mosaic of characters that we find in *Au. sediba* suggest that taxonomically assigning fragmented or isolated remains can be hazardous.

## TEXT S2. An updated stratigraphy and sedimentology

The Malapa site in the Cradle of Humankind world heritage area occurs in the valley of the Grootvleispruit, in chert-poor dolomite of the Lyttelton Formation (3). The site represents a deeply eroded cave chamber 15-20 m in diameter, which is partly exposed in several shallow pits, originally dug by miners looking for calcite, in the form of thick speleothem deposits, within caves. The main one of these pits (Pit 1) has been described in (3) and contains well-preserved fossil remains of *Au. sediba* (2).

(3) presents a stratigraphy for the cave deposits encasing the fossils of *Au. sediba*, and provides a description of the various lithofacies encountered in the deposits in Pit 1. During surface excavations of the Malapa site in March 2010, soil cover, mixed with fossil-bearing scree, was removed from the top of part of the cave system, to expose new outcrops of fossil-bearing cave deposits in a shallow pit (Pit 2) and a series of large dolomite blocks and consolidated cave sediment blocks, which represent the remains of a palaeo-roof collapse (Figs. 1 and 2) and known as Pit 2. The excavations also exposed a speleothem deposit (Flowstone 2) positioned stratigraphically above the main fossil-bearing unit, as discussed in the main text of this paper.

Apart from the removal of surface material, large blocks of fossil-bearing carbonaceous sandstone were removed from Pit 1, providing new exposures along the N and E face of the pit. Presented below is an updated description of the stratigraphy and cave facies as exposed in both Pit 1 and 2 on 18 November 2010 (Fig. 1). Rock facies that were described in (3) have been briefly summarized. Adjustments and expansions to the earlier stratigraphy and facies descriptions are provided in more detail in Table S1.

<b>Facies Name</b>	<b>Up-dated description</b>	<b>Sedimentary environment</b>
Facies A*	Dark-colored, moderately sorted, coarse-grained clastic sediment, abundant rounded clastic grains (0.5-6 mm), ooids, bone fragments and peloids.	Facies A was water-laid and deposited along a fluvial channel.
Facies B*	Peloidal grainstone, rich in fenestrae along bedding planes, alternating with clastic sandstone rich in ooids, rounded chert/quartz grains, shale and bone material, insect burrows are common. Small stalagmite bosses growing on a grainstone substrate, and isolated dolomite blocks (<40 cm).	Facies B was deposited along a muddy cave floor, with local speleothem deposition. Flowing water provided incursions of clastic sediment and washed in faunal remains.
Facies C	Variation of the peloidal grainstone units in Facies B, but is homogenous and lacks clastic intercalations. Rich in fenestrae, which define the primary layering. The top of this block consists of a porous sugary, 8cm thick layer composed of ~50% spherical mud pellets ~35% sparite and ~15% voids. The mud pellets show a coarsening-up trend, and form a loosely packed framework that is partly filled with coarse-grained, isopachous sparite cement (Figs. 1 and 2).	Facies C represents mud which accumulated partly as peloids along the base of cave chambers. The fenestrae indicate that the mud was rich in organic material. Isopachous sparite cement formed in a waterlogged environment in a cave chamber that occurred at a higher level than the chamber in which the <i>Au. sediba</i> fossils were buried.
Facies	Massive unit consists of a poorly sorted,	Deposited as a water-logged mass flow

D	coarse-grained sandstone cemented by blocky sparite. The top 30 cm of Facies D contain fossil remains of MH1 and preserve a weak horizontal layering defined by a gradual fining-upward of the sandstone, and a weak alignment of clastic elements, clearly visibly in scans of the braincase of MH1.	deposit carrying with it a number of specimens of <i>Au. sediba</i> (3).
Facies E	Calcareous sandstone, similar to Facies D, but darker colored, and finer-grained, with a higher degree of sorting and rounding, and preserving 4-15 cm scale horizontal layering. The basal layer consists of well-sorted, coarse-grained sandstone, which is locally in sharp contact with the rocks of Facies D.	The change from Facies D to Facies E reflects a change to lower flow regimes from high velocity mass flow to alluvial flow of variable strength.
Facies F	Fine-grained massive rock preserving a crude layering defined by alternating peloidal grainstone and sandy peloidal grainstone layers. Differs from Facies B in that it does not contain sandstone intercalations, and speleothem build-ups, and it contains a higher proportion of fossil material and large blocks of dolomite.	Partly disintegrated epifossils form a dark-brown muddy matrix, indicating the sediments were waterlogged, whilst fossil bone shows abundant evidence of water damage.

**TABLE S1:** Summary of Malapa facies descriptions and their corresponding depositional environments. (\*=unchanged from original description in (3)).

**Facies relationships and updated stratigraphy.** Facies A and B represent the oldest sediment layers preserved at the site and their descriptions remain unchanged from (3). Facies C was originally described as being preserved as a 5-30 cm thick erosion remnant that drapes flowstone 1 in the NW corner of the main pit (3). Removal of some large blocks along the NW wall shows that Facies C actually occurs as a thin erosion remnant between dolomite forming the western sidewall of the pit and rocks belonging to Facies B, a laminated flowstone-sandstone unit, and exposure of Facies E (and perhaps D), which on-lap onto the erosion remnant as shown in the schematic cross-section in Fig. 2. Facies C also occurs as remnants on top of the largest of the roof blocks (Block 2) occupying the centre of the excavation. The top-most roof block; i.e. Block 3 covered by the upper flowstone unit, also consist of Facies C. Facies D overlies flowstone 1 in the center and east of the pit and a laminated sandstone-flowstone unit described below. It possibly sits unconformably on Facies C along the west-wall of the pit, but exposure is poor. The fossil material belonging to MH1 occurs within the layered sediments of Facies D indicating that the fossil was partly reworked in these sediments, or that the sediments were building up around the fossil remains. Along the NE and E wall of the cave the transition from massive sandstone (Facies D) into layered sandstone (Facies E) appears gradational.

The fact that MH1 is well preserved in both Facies D and Facies E suggests that these two rock types were deposited in quick succession, and that the layered sediments of Facies E accumulated soon after the mass flow with fossils was dumped in the bottom of the cave. Facies F was described by (3) as the finer-grained top of Facies E, but has now been identified as a separate facies, occurring within a distinct stratigraphic unit. In the NE corner of Pit 2, a 20 cm sized block shows clear evidence of having

fallen into, and deformed primary layering indicating that Facies F formed as a thick, semi-consolidated and water-logged build-up of mud. At the time the cave chamber would have been a deep cavern floored by mud and pooling water allowing clastic material to fall in on occasion, but not regularly.

The various cave facies described occur in rocks that can be divided into at least 4 distinct stratigraphic units separated by unconformities, event horizons or periods of flowstone formation. The oldest unit in Pit 1 is represented by grainstone of Facies C, which occurs as remnants unconformably covered by flowstone drapes and rocks belonging to Facies B and E (and possibly D). The next conformable package of rocks is that consisting of Facies A and Facies B type rocks underlying Flowstone 1. These rocks were eroded before they were covered by the flowstone intercalated with incursions of fossil-bearing clastic sediment. The next stratigraphic unit consists of the mass-flow deposits of Facies D and the layered water-laid sediments of Facies E. This unit contains abundant hominid material and was probably deposited in a short time period to explain the exquisite preservation quality of many of the fossils. The unit was covered by a roof collapse which occurred before Facies E had fully consolidated considering the evidence for soft-sediment deformation described in the main text. After roof collapse flowstone formation continued for some time, before a muddy unit represented by Facies F accumulated.

### TEXT S3. Updated magnetostratigraphy for the Malapa site

The palaeomagnetic data is presented in Table S1 and representative samples are shown in Fig. S2. ). As noted in (3), South African samples are often dominated by ultra-fine grained magnetite across the single domain (SD) to superparamagnetic (SP) grain sized boundary. This is due to repeated erosion and burning of the landscape which creates a large number of easily remagnetised grains. This grain size carries a secondary overprint which needs to be carefully removed to identify the primary remanence that was formed in the sample close to its time of deposition. As described (3), the remanence in the samples is predominantly carried by magnetite as shown by the Curie points of 550-570°C (Fig. S3). However, the presence of maghaemite is also detected based on a thermal transition at ~150°C in the thermomagnetic curves and a decrease in magnetization on cooling (Fig. S3C). This is most likely due to low temperature oxidization during weathering. However, there is no suggestion of multi-domain (MD) grains based on low temperature magnetic susceptibility curves (Fig. S3D). A MD peak, or even a suppressed peak due to low temperature oxidization is not noted in any of the Malapa samples. The mixed SD and SP character (SP tail; Fig. S3D) of the low temperature curves adds further evidence that the low coercivity (Fig. S3B) of the samples is caused by a large proportion of strong ferromagnetic grains across the SP to SD grain-sized boundary. True SP grains do not hold a stable remanence and the grains at the SP to SD grain sized boundary are susceptible to repeated short term remagnetization as shown by the strong, but easily removed, isothermal overprint occurring in the samples due to sampling, transport and preparation of the samples. This is indicated by the change in the overprints character after only short term storage in a zero field cage at the laboratory. The ChRM is carried in larger stable single domain grains as shown by a lack of saturation of IRM curves until close to 300mT (Fig. S3A). This is a typical character of the South African sites and this grain size is capable of holding a stable geological remanence close to the time of deposition. The reliability of the palaeomagnetic data is further supported by the cross correlation of geomagnetic field polarity with other relative and chronometric methods at a range of South African sites (62).

To better isolate the underlying characteristic remanence (ChRM). Sediment samples were subjected to a combination of thermal (TH), alternating field (AF) and a hybrid (AF/TH) method of alternating field followed by thermal demagnetization as outlined in (3). Speleothem samples were only subjected to AF and hybrid demagnetization due to expansion of the calcite and cracking at higher temperatures due to fluid inclusions. Samples were heated in a Magnetic Measurements thermal demagnetizer and measured on an AGICO JR6 magnetometer within a zero field cage. Mineral magnetic measurements were run on a Magnetic Measurements variable field translation balance (VFTB).

[insert Fig S2]

The samples generally record a strong overprint that is removed by fields of 10-15mT to record an underlying stable characteristic remanence (ChRM) that can be both normal and reversed in polarity (ChRM; Fig. S2). Multiple samples from the same blocks show similar demagnetization spectra and record the same polarity using all three methods of demagnetization and isolation of the ChRM (see PM04 and PM09 in Fig S2). The ChRM is suggested to represent the remanence formed in the sample soon after deposition. Lower K values for some samples relate to the fact that the remanence recorded is a post-depositional remanence formed soon after deposition due to de-

watering and compaction of the sediments. In contrast, the remanence recorded in the Malapa speleothems is a detrital origin depositional remanent magnetization that is locked in almost instantly after deposition (63). In speleothems any scatter is due both to the weakness of the samples and the fact that more than one layer of flowstone is being measured in one sub-sample. However, due to the strong detrital nature of the remanence carried in the speleothems it has been possible to identify changes in direction in different layers through the same block sample. As such, the sequence in the thick flowstone sample PM01 has been expanded upon since (3) by measuring the flowstone in finer resolution. On removal of the IRM and any viscous remanence the samples are stable to both alternating field and thermal demagnetization up to 50mT or ~550°C. This is a common character for samples from the South African caves (14, 64).  
[insert Fig S3]

The palaeomagnetic analysis used to constrain the age of the Malapa cave sediments and speleothem is based on the changing polarity of the Earth's magnetic field, which in the past has happened numerous times and on a number of different time scales (15, 65, 66). The last long-lived geomagnetic field change occurred ~0.780 million years (Ma) ago (66). In addition to long-lived changes, a number of short events and excursions have also occurred throughout Earth's history, some lasting as little as 3,000 to 20,000 years (15, 65).

The speed of sediment infill of the caves varies considerably from site to site and from different parts of the same cave system. While massive australopith-rich breccia talus cones, such as Sterkfontein Member 4, formed primarily via collapse and over long time periods (~600,000 years) (1, 14, 62), fluvial sandstone, siltstone, and mudstone deposits accumulated more rapidly (1, 3) and are likely to preserve more complete skeletons. When cave deposits form continuously over a short period of time they may preserve a high resolution palaeomagnetic record that holds the potential to preserve short-lived geomagnetic field events, as can sometimes be recorded in lake sediments (67). A number of studies indicate that these short geomagnetic field events can be accurately recorded within speleothems of the South African Plio-Pleistocene palaeokarst. Flowstones, as with most speleothems, are inherently amenable to U-Pb dating and recently have been used to date three hominin-bearing cave sites close to Malapa (8, 14, 17). Identifying these events within U-Pb dated flowstones or within sediments associated with them holds the potential to produce extremely accurate ages for fossil bearing deposits in caves.

A fully reversed, normal polarity event has been identified and dated in two flowstones, one at Malapa ( $2.026 \pm 0.021$  Ma; 2.047-2.005 Ma) (3) and one at Sterkfontein ( $2.014 \pm 0.055$  Ma; 2.069-1.959 Ma) (1, 14, 62). Taken together this data suggests this event dates to sometime between 2.05 and 2.01 Ma, consistent with previous age estimates of an event (Huckleberry Ridge) at ~2.06-2.02 Ma (18, 68). The Huckleberry Ridge Tuff itself has been re-dated to  $2.059 \pm 0.004$  Ma (2.063-2.055 Ma; 69), slightly older than the South African event. Moreover, the Huckleberry Ridge Tuff contains transitional directions, unlike those from the South African speleothem (69). On Réunion island two events/excursions are recorded, the older Réunion event has been dated to  $2.15 \pm 0.02$  Ma and has fully reversed directions, while the younger excursion has been dated to  $2.04 \pm 0.02$  Ma (2.06-2.02 Ma; 68). The dipole intensity decrease was not as pronounced during this younger excursion and as such it does not occur as a 180° directional change in many part of the world, but appears as a geomagnetic excursion during an episode of increased secular variation (68). Given that the South African event is older than the Huckleberry Ridge Tuff excursion and fully reversed, there is the possibility that the Huckleberry Ridge Tuff does not fully record

the event but just the beginning or that it is an older excursion. The reversal at the base of the normal polarity event is not recorded in the Malapa flowstone. However, this is not the case at Sterkfontein, where the age of  $2.014 \pm 0.055$  Ma (2.069-1.959 Ma) dates the flowstone just under the normal polarity event itself. The age of  $2.059 \pm 0.004$  Ma for the Huckleberry Ridge Tuff is a mean Ar-Ar age (69). Two total fusion Ar-Ar samples produced ages of  $2.050 \pm 0.010$  and  $2.050 \pm 0.016$  Ma (2.066-2.034 Ma), much more consistent with the U-Pb ages from South Africa (2.047-2.005 Ma) (69). Moreover, previous total fusion Ar-Ar ages also gave more consistent results of  $2.037 \pm 0.008$  Ma (2.045-2.029 Ma; 69) as did Ar-Ar incremental heating experiments  $2.060 \pm 0.011$  Ma -  $2.049 \pm 0.011$  Ma (2.071-2.038 Ma; Plateau age) and  $2.062 \pm 0.023$  Ma -  $2.049 \pm 0.012$  Ma (2.085-2.037 Ma; isochron age; 69). As such the normal polarity reversal noted in the Sterkfontein and Malapa flowstones (2.05 and 2.01 Ma) is consistent with being the Huckleberry Ridge event dated elsewhere and can be constrained to between 2.05 and 2.03 Ma based on all ages for this event. Two distinct geomagnetic field events appear to be recorded in the Sterkfontein flowstone post  $2.014 \pm 0.055$  Ma (14). This may relate to variability within the Huckleberry Ridge event or the younger of these events may relate to the Pre-Olduvai event at 1.977 Ma (18). Other events, such as the Blake event, show similar 'double event' characters (67). This adds further weight to the body of evidence that suggests a high degree of instability of the magnetic field between ~2.25 and 1.95 Ma, just prior to the Olduvai Subchron.

Flowstone 1 in Pit 1 consists of a single sheet in the SE corner of the pit, and splits in two and then three separate sheets towards the center of the pit where the top sheet directly underlies MH2. The three sheets are separated by layers of fossil-bearing sandstone and siltstone units, which increase in thickness from SE to NW. (3) describes palaeomagnetic samples taken from each of the three layers. The basal layer of Flowstone 1 (PM01) records stable normal polarity at its base followed by intermediate polarity and then reversed polarity. The laser ablation U and Pb concentration profiles for flowstone sample PM01 and sample M1 (taken from the W-side of the pit dated at 2.026 Ma (3) shown in SOM fig. S1 can be used to correlate these two samples and indicate that these two samples are sourced from the same layer.

[insert Fig S1]

The normal polarity in the base of the speleothem is interpreted as representing the Huckleberry Ridge event (3) at ~2.05-2.03 Ma. The middle (PM03) and upper (PM02) flowstone layers record stable reverse polarity of the Matuyama Chron (2.03-1.95 Ma). The top and middle flowstone layers cannot be correlated directly with flowstone along the west wall of the pit, but thin out and disappear (Fig. 2). Instead, in a lateral up-dip position from the flowstone along the NW corner of the pit a finely laminated unit occurs that is composed of mm-scale sandstone-siltstone layers with abundant, angular clastic fragments (mainly dolomite, chert and speleothem) intercalated with regular 0.1-1.0 mm-thick drapes of flowstone, which appears to stratigraphically accumulate on top of the topmost massive flowstone sheet by as much as 30 cm. The top of the laminated sandstone-flowstone unit constitutes the base of paleomagnetic sample PM04 (originally the rocks above the limited flowstone were identified as Facies C in (3); however they have now been identified as the finer-grained, weakly layered top of Facies D), 25 cm below the in situ foot bones of MH1, and about 30 cm, stratigraphically above the position of the top flowstone layer where this layer thins into a thin drape. The laminated sandstone-flowstone unit also constitutes paleomagnetic sample PM09. A thin flowstone layer in the base of PM04 (base) and PM09 record normal polarity (3; Table S1) and are overlain by clastic sediments that belong to the weakly layered top of Facies D or the layered base of

Facies E, thus the laminated sandstone-flowstone unit represents a distinct stratigraphic horizon with normal magnetic polarity positioned above the massive flowstone unit (with reverse polarity), but below sediments of Facies D and E. The sediments in the top of PM04 (top of Facies D) and sediments from Facies D (i.e. PM05 in (3)) record intermediate and normal polarity.

Site	Deposit	Sample	Dec.	Inc.	K	No.	P.Lat.	Polarity	Chron/excursion	Age (Ma)	U-Pb (Ma)
UW88	Flowstone	PM10	193	48	199	6	-80	R	MATUYAMA	>1.95	1.975 ±0.142
UW88	D	PM05A	214	-1	36	4	-48	I	T		
UW88	D	PM05B	343	-47	19	3	73	N	PRE-OLDUVAI	1.977	
UW88	D	PM09A	18	-42	29	6	72	N	PRE-OLDUVAI	1.977	
UW88	D	PM09B	338	-39	79	5	70	N	PRE-OLDUVAI	1.977	
UW88	D	PM04A	39	-6	296	6	46	I	T		
UW88	D	PM04B	30	-41	78	2	63	IN	T		
UW88	Flowstone	PM02	191	48	47	6	-80	R	MATUYAMA		
UW88	Flowstone	PM03	188	50	34	6	-79	R	MATUYAMA		
UW88	Flowstone	PM01A	157	48	87	3	-70	R	MATUYAMA		
UW88	Flowstone	PM01B	200	-84	58	2	14	I	T		
UW88	Flowstone	PM01C	307	-73	298	2	41	I	T		
UW88	Flowstone	PM01D	20	-57	56	4	71	N	H. RIDGE	~2.04	2.026 ±0.021

**Table S2.** Palaeomagnetic data from the Malapa deposits

[insert Fig S4]

Since (3) additional sub-samples were taken from PM05, PM09 and PM04 as well as throughout flowstone PM01. Due to the strong remanence recorded in these sediment samples it was possible to take very small cores from the blocks (1 cm<sup>2</sup>) and so avoid any large clasts that occasionally occur within the samples. Large clasts were a particular problem of sample PM09. It was not possible to take additional clastic samples at this stage as the fossil deposits within the cave are so dense there is a danger of damaging in-situ hominin fossils. However, the size of the original blocks taken did allow multiple layers of deposits to be analyzed independently. For example, the base of PM04 is a thin intermediate normal polarity flowstone. Intermediate polarity directions, but heading in the direction of a normal polarity (positive Pal.Lat) in the top, clastic portion of PM04 could be due to post-depositional inclination shallowing related to dewatering and compaction of the sediments, which would otherwise have recorded a normal polarity. However, this is not the case for flowstones where the remanence is locked in on precipitation of the flowstone. In all cases the remanence in flowstones is due to clastic inclusions rather than a precipitated remanence. Remanence appears to have been locked in early on in some sediment sample, notably PM09, due to the stabilizing effect of very thin flowstone layers. These two samples thus indicate the presence of both intermediate to normal polarities during the deposition of the *Au. sediba* bearing clastic deposits.

Originally these normal polarity directions were interpreted as representing the Olduvai SubChron between 1.95 and 1.78 Ma (3). However, a new speleothem sample (PM10) was taken from a flowstone capping the normal polarity *Au. sediba* bearing

deposits. PM10 records a reversed polarity (Fig. S4) and has been U-Pb dated to  $1.975 \pm 0.142$  Ma (2.12-1.83 Ma). Given this age the reversed flowstone PM10 must be older ( $>1.95$  Ma), rather than younger ( $<1.78$  Ma) than the Olduvai Subchron. The normal polarity directions of the *Au. sediba* bearing sediments must therefore also be older than 1.95 Ma, but younger than the Huckleberry Ridge event at 2.05-2.03 Ma. The pre-Olduvai excursion (17) at 1.977 Ma is the only validated or suggested excursion between the Huckleberry Ridge event at 2.05-2.03 Ma and the Olduvai sub-Chron at 1.95 Ma (15). This event has also been potentially identified in lacustrine sediments below the KBS tuff at Illeret in Kenya (70) and flowstone at Sterkfontein, however, the Malapa data is the best terrestrial evidence for this reversal, which had previously only been noted in deep sea sediment cores (18). The pre-Olduvai excursion is estimated at around 3 ka in duration (18) and suggests the sediments accumulated rapidly at  $1.977 \pm 0.002$  Ma.

The Malapa sequence indicates the potential for cave sediments to record short geomagnetic events and excursion and the ability to date them if occurring within or in close association to speleothems. However, it also shows the complexity of undertaking magnetostratigraphic analysis of such deposits and the potential for misinterpretation of polarities to the wrong Chron or Sub-Chron in the absence of precise stratigraphic control and detailed absolute age dating. The sequence outlined in (3) was the most parsimonious situation given the underlying speleothem age. However, with new dates on the capping speleothem and the re-interpreted stratigraphy the sequence outlined above is considered the most likely.

In conclusion, geological evidence suggests that the deposition of the hominid-bearing sediments of Facies D and E was sudden and occurred over a short period of time spatially and temporally closely associated, and perhaps related, to the collapse of the cavern in which the fossils were buried. If so, formation of the top flowstone could be seen as a continuation of deposition of the basal flowstone, with the fossil-bearing sediments and the roof blocks representing some sort of event horizon, possibly triggered by the influx of large amounts of water into the cave. The available evidence suggests that this event coincides with a short period of normal polarity, which, considering the U-Pb dates coincides with the  $\sim 1.977$  Ma pre-Olduvai excursion providing a remarkably accurate and internally consistent age estimate for the *Au. sediba* fossils MH1 and MH2.

#### TEXT S4. U-Pb dating: material, methods and results

Flowstone 2 in the newly exposed portion of the Pit 2 was sampled in two locations for U-Pb dating (samples M6 and M7; Fig S4). A significant challenge to the U-Pb dating of speleothems is presented by the abundances of both U and Pb within samples. For samples with less than around 1 µg/g of U, radiogenic Pb in growth is very low, and incorporation of large proportions of so-called ‘common’ Pb will also swamp any radiogenic signature. As a consequence any method to detect ‘U-rich’ layers prior to analysis is indispensable (17, 71, 72). Our samples were pre-screened with laser ablation inductively coupled mass spectrometry (ICPMS) traverses; U and Pb concentrations are plotted relative to an image of the samples in Fig. S5. Both M6 and M7 present clearly defined layers with enhanced U-content, up to 1cm thick, located near the base of the flowstone horizons (Fig. S5).

[insert Fig S5]

Full analytical details of the method used can be found in (16) and (17) and are therefore only briefly reported here. Using the laser ablation information noted above U-rich layers are selected and up to 10 ~0.05 g blocks are cut from each sample, ideally from within a single growth layer (although this is not always possible) using a dental drill. After a brief leach to remove any surficial contamination, samples are dissolved in HCl, spiked with a  $^{233}\text{U}$ - $^{205}\text{Pb}$  tracer and U and Pb separated by conventional ion exchange techniques. A double-focusing Nu Instruments® MC-ICP-MS was used for all isotopic measurements. We used the NIST SRM 960 and NIST SRM 981 reference materials to tune machine settings and to monitor and correct for instrumental isotope fractionation (in the case of Pb; for U mass fractionation was corrected using the sample  $^{235}\text{U}$ - $^{238}\text{U}$  ratio). While U blanks are negligible, Pb blanks for the period of these analyses averaged 10pg and appropriate blank corrections have been performed.

Uranium concentrations in the samples are typically ~0.4 µg/g, while Pb concentrations are on average thirty times lower in the ng/g range (Table S3).  $^{206}\text{Pb}/^{204}\text{Pb}$  ratios show limited variation, ranging from 18 to a little over 22. Because of this limited range in the Pb isotope ratios, we plotted all the analysis for samples M6 and M7 onto a single Tera-Wasserberg concordia diagram, to allow for the maximum spread of the data and the best defined slope. We are confident that the two samples M6 and M7 are originally from the same flowstone layer, as their U and Pb profiles (measured through the laser ablation analysis (Fig S5) are very similar. The U and Pb profile of Flowstone 1 (Fig S1) share no similarities with those from M6 and M7, further strengthening the case that Flowstone 2 formed at a distinct, later time than Flowstone 1.

The resulting MSWD is considerable at 606 and reflects the large scatter of the points away from the slope due to variability in the isotopic composition of the common Pb component. The linear regression through these points was calculated using an *Isoplot* “Model 2 fit” (Fig S6; 73), in which their scatter about it is uniform and is taken as the per data point uncertainty. The large number of analyses in the regression allow for a confident determination of this degree of scatter and thus of the uncertainty on the regression itself. (Fig S7). Selective removal of points from the regression results in very little change to the final age estimate, and all data have been included

[Insert Fig S6, S7 and Table S3]

Age calculations using the  $^{238}\text{U}$ - $^{206}\text{Pb}$  and  $^{235}\text{U}$ - $^{207}\text{Pb}$  decay chains are complicated by their initial disequilibrium. Initial  $^{231}\text{Pa}/^{235}\text{U}$  and  $^{230}\text{Th}/^{238}\text{U}$  are presumed to be zero

but initial  $^{234}\text{U}/^{238}\text{U}$  must be constrained in some way. In the case of an initial ( $^{234}\text{U}/^{238}\text{U}$ ) activity ratio of  $\approx 1.3$  a simple isochron construction leads to an overestimate of the sample age because it does not take into account  $^{206}\text{Pb}$  produced from the decay of excess initial  $^{234}\text{U}$ . Present day residual  $^{234}\text{U}/^{238}\text{U}$  ratios were measured on large ( $>150\text{mg}$ ), representative sub-samples from each of the dated layers; the results of these measurements are provided in column five of Table S3 under the heading ‘present day  $^{234}\text{U}/^{238}\text{U}$ ’. (17) (Table S2) and from these data a correction can be made for the effects of initial isotopic disequilibrium of intermediate daughter products of the U decay chain. Great care was taken to sample the same time horizon for the isochron samples and the ( $^{234}\text{U}/^{238}\text{U}$ ) measurement. The uncertainties of the ( $^{234}\text{U}/^{238}\text{U}$ ) measurements easily explain the observed difference in ( $^{234}\text{U}/^{238}\text{U}$ ) between growth layers, meaning we can be confident that a weighted average of the ( $^{234}\text{U}/^{238}\text{U}$ ) measurements is representative of the whole layer. If there is greater scatter in the  $^{234}\text{U}/^{238}\text{U}$  at the smaller sampling scale, we feel that this is covered by the very conservative uncertainties associated with our  $^{234}\text{U}/^{238}\text{U}$  measurements. As we combined the U-Pb data for samples M6 and M7, we used a weighted average of the two  $^{234}\text{U}/^{238}\text{U}$  measurements, which brings the ( $^{234}\text{U}/^{238}\text{U}$ ) measured to  $1.0076 \pm 0.0030$ .

Final ages are calculated by using the Tera-Wasserberg isochron construction, employing  $^{238}\text{U}/^{206}\text{Pb}$  vs  $^{207}\text{Pb}/^{206}\text{Pb}$  ratios (73) and following the disequilibrium correction methods described in (16) (Fig. S6, S7). Our final age error of  $\pm 140$  ka takes into account the scatter on the isochron, and the effect of the initial  $^{234}\text{U}$  disequilibrium on the age, as well as the uncertainties associated with its measurement. Monte-Carlo modelling of the  $^{207}\text{Pb}/^{206}\text{Pb}$ – $^{238}\text{U}/^{206}\text{Pb}$  isochron intercept with the measured  $^{234}\text{U}/^{238}\text{U}$  disequilibrium-corrected concordia (Fig S8) shows that uncertainties are symmetric about the mean value, with respect to the significant figures shown. The final U-Pb age for Flowstone 2 (Fig. S6) is relatively precise, with a 7% error, which is typical for the cave sites in the Cradle of Humankind (1, 8).

[insert Fig. S8]

It should be noted that the uncertainty of our linear regression is very large as expected from the scatter of the data ( $\pm 15\%$  at the concordia intercept; Fig S7), but that uncertainty on the final age is effectively half of this through the constraining effect of the measured  $^{234}\text{U}/^{238}\text{U}$  disequilibrium on the corrected age (Fig S8).

When the U-Pb age estimate, stratigraphy and palaeomagnetic results are combined, an age of 1.977 Ma provides the best possible explanation of all the available data.

## Figure Captions

**Fig. S1.** U and Pb concentration profiles for flowstone samples PM01 and M1 used to correlate these two samples.

**Fig. S2.** Demagnetization spectra for reversed flowstone sample PM10, normal polarity thin flowstone sample PM04B, intermediate polarity sediment sample PM04A and normal polarity sediment sample PM09B. Three sub-samples are shown overlapped for layer PM04B and PM09B and show the consistency of the paleomagnetic directions between sub-samples. For PM04B thermally demagnetized (TH) and hybrid demagnetized (AF-TH) samples are compared. PM10 and PM04 show examples of alternating field demagnetized samples.

**Fig S3.** Mineral magnetic measurements of sample PM04 from Malapa. A) IRM acquisition curve; B) Hysteresis loop; C) Thermomagnetic Curve; D) Low temperature magnetic susceptibility curve ( $10^{-5}$  SI).

**Fig S4.** Photograph of the newly exposed flowstone layer at Malapa (A) with the locations of U-Pb samples M6 (C) and M7 (B), and new palaeomagnetic sample PM10 (D), scale bars 10cm.

**Fig. S5.** Laser ablation U and Pb concentration profiles plotted against flowstone samples M6 and M7 with areas targeted for dating marked with a dashed box.

**Fig S6.** Tera-Wasserberg age plot for Flowstone 2.

**Fig S7.** Extrapolated view of the linear fit of fig S6, showing its  $2\sigma$  uncertainty envelope and intercept with disequilibrium concordia for  $[\text{}^{234}\text{U}/\text{}^{238}\text{U}]_i$  of 2.73, 3.47 and 4.23. The green dots are a 1000-point Monte-Carlo simulation of the disequilibrium-corrected age.

**Fig S8.** Expansion of the disequilibrium concordia (black) intercept of the linear fit to data (red) of Fig S7. Measured  $[\text{}^{234}\text{U}/\text{}^{238}\text{U}]$  is in blue, and disequilibrium isochrons in grey. The disequilibrium concordia and isochrons depicted are outputs of a 1000-point Monte-Carlo simulation (green), which took the linear fit and measured  $[\text{}^{234}\text{U}/\text{}^{238}\text{U}]$  as its inputs.

Sample	U ppm	Pb ppm	$\frac{^{238}\text{U}}{^{206}\text{Pb}}$				corr. coef. 8/6- 7/6	$\frac{^{238}\text{U}}{^{204}\text{Pb}}$				corr. coef. 8/4- 6/4	Present $^{234}\text{U}/^{238}\text{U}$			U-Pb (T-W) age (Ma)			Initial $^{234}\text{U}/^{238}\text{U}$	
			% err	$\frac{^{207}\text{Pb}}{^{206}\text{Pb}}$	% err	% err		% err	% err	% err	$\pm$		% err	2SE	% err	$\pm$				
M6-1	0.28	0.019	51.4	1.0	0.8068	0.1	-0.951	1002.1	1.1	19.51	0.2	0.820				2.048	0.140	7	3.51	0.86
M6-2	0.39	0.010	127.2	1.5	0.7797	0.2	-0.999	2581.9	1.8	20.30	0.3	0.894								
M6-3	0.38	0.013	99.1	1.2	0.8113	0.1	-0.854	1932.9	1.4	19.50	0.5	0.601								
M6-4	0.31	0.053	19.4	0.4	0.8388	0.03	-0.876	360.5	0.4	18.56	0.1	0.640								
M6-5	0.29	0.020	47.5	0.8	0.8098	0.1	-0.943	922.4	0.9	19.40	0.2	0.790								
M6-6	0.35	0.009	132.8	1.6	0.7813	0.3	-0.977	2676.0	1.9	20.16	0.4	0.812								
M6-7	0.30	0.023	42.7	1.2	0.8012	0.2	-0.983	838.9	1.3	19.64	0.2	0.851								
M6-9													1.0065	0.0042	0.4					
M7-1	0.46	0.004	342.1	3.8	0.7138	1.0	-0.997	7674.8	5.0	22.44	1.3	0.964								
M7-2	0.47	0.008	181.6	1.7	0.7812	0.3	-0.999	3630.6	2.0	19.99	0.4	0.844								
M7-3	0.47	0.011	139.6	3.1	0.7854	0.5	-0.990	2772.9	3.6	19.87	0.7	0.835								
M7-4	0.47	0.006	265.1	4.2	0.7397	1.0	-0.993	5731.9	5.4	21.62	1.3	0.908								
M7-5	0.48	0.009	177.8	2.4	0.7818	0.4	-0.999	3574.2	2.9	20.11	0.5	0.853								
M7-6	0.74	0.008	313.3	3.6	0.7246	0.9	-0.999	6946.0	4.7	22.17	1.2	0.958								
M7-8	0.46	0.006	255.3	2.9	0.7396	0.7	-0.999	5368.4	3.6	21.03	0.8	0.910								
M7-9													1.0086	0.0042	0.4					
Ave.	0.42	0.014											1.0076	0.003	0.3					

**Table S3.** All data needed to calculate U-Pb ages, unspiked  $^{234}\text{U}/^{238}\text{U}$  values and Terra-Wasserberg plot U-Pb ages for Malapa flowstones.

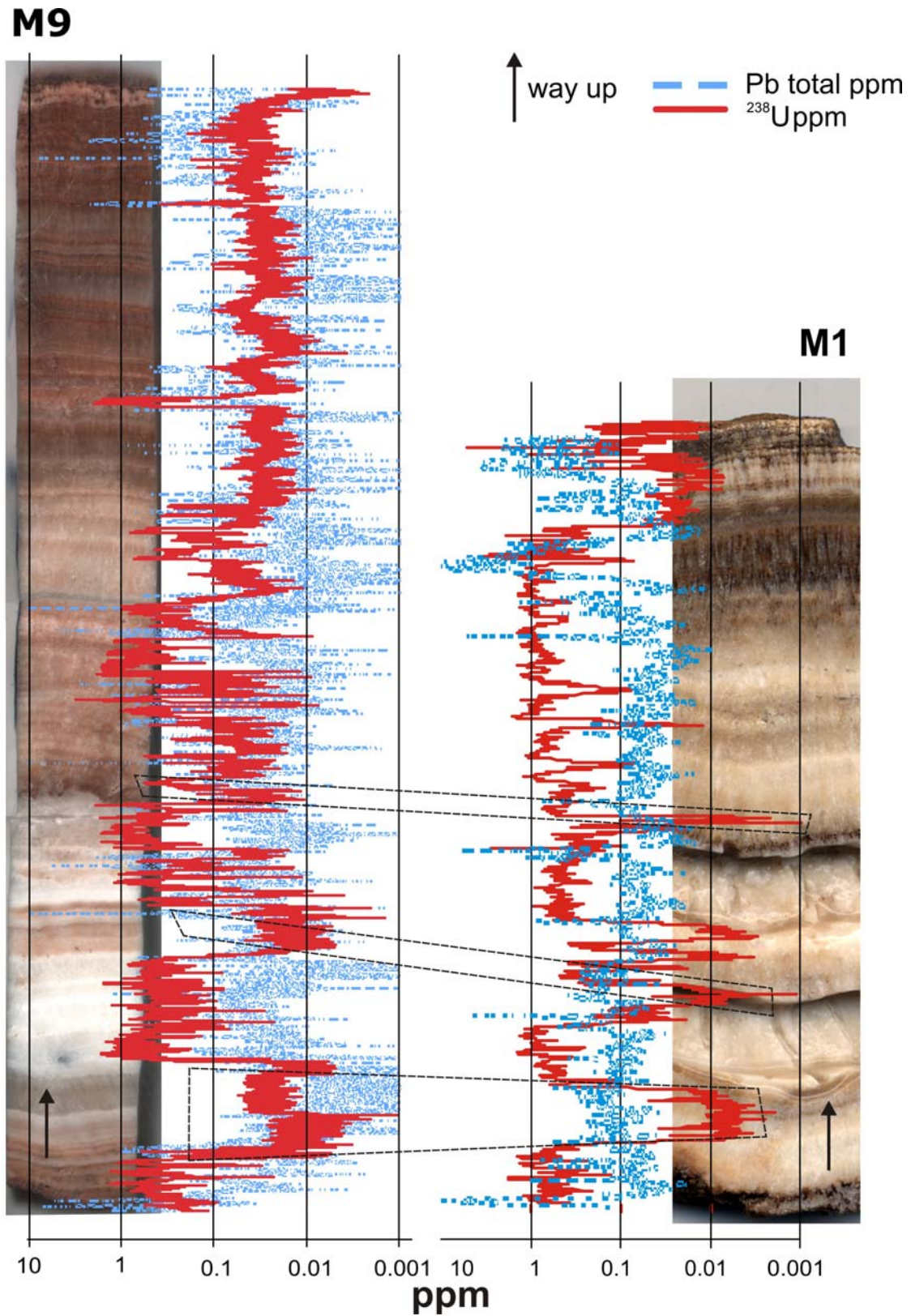


**Fig. S1.** U and Pb concentration profiles for flowstone samples PM01 (M9) and M1 used to correlate these two samples.

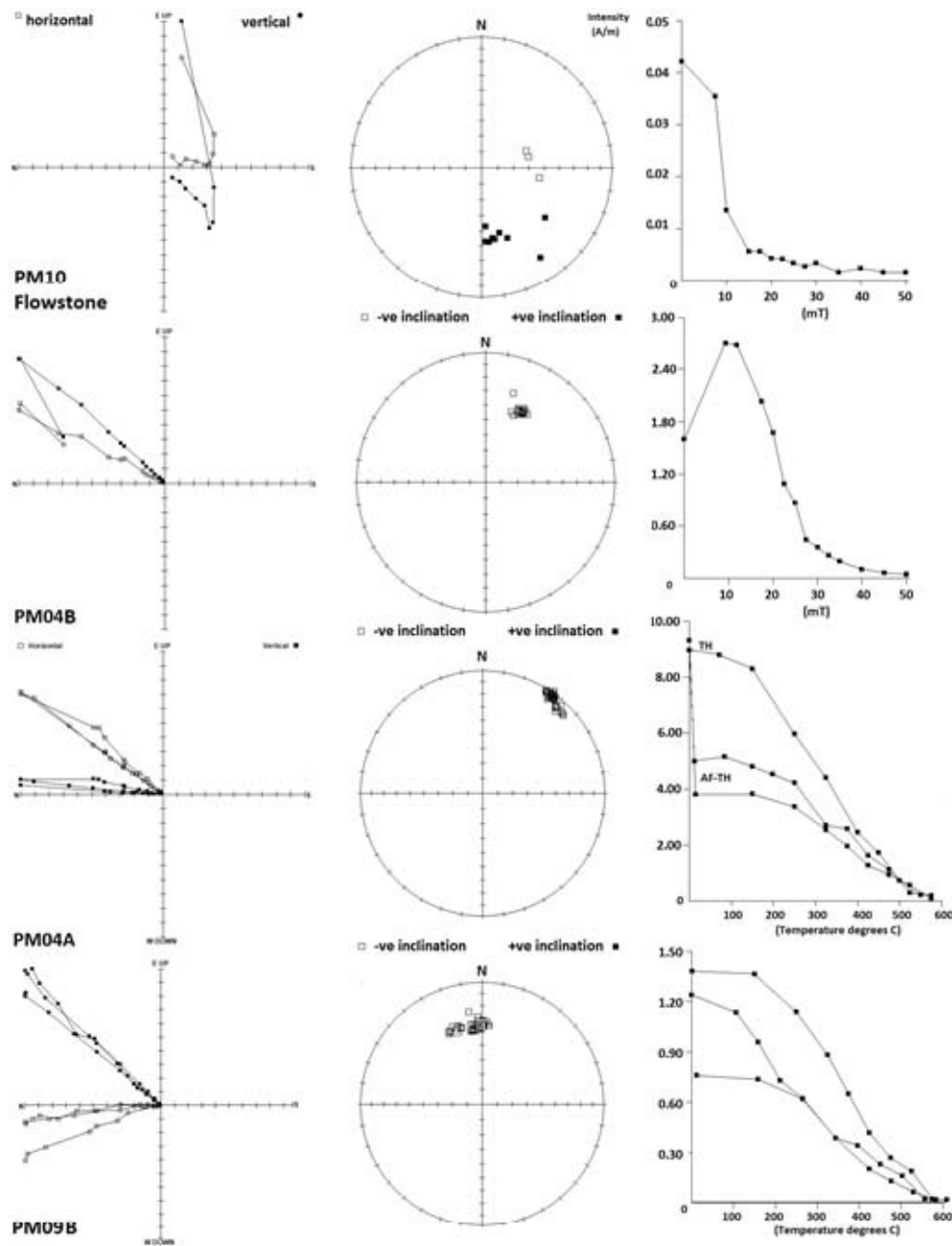


**Fig. S2.** Demagnetization spectra for reversed flowstone sample PM10, normal polarity thin flowstone sample PM04B, intermediate polarity sediment sample PM04A and normal polarity sediment sample PM09B. Three sub-samples are shown overlapped for layer PM04B and PM09B and show the consistency of the paleomagnetic directions between sub-samples. For PM04B thermally demagnetized (TH) and hybrid demagnetized (AF-TH) samples are compared. PM10 and PM04 show examples of alternating field demagnetized samples.

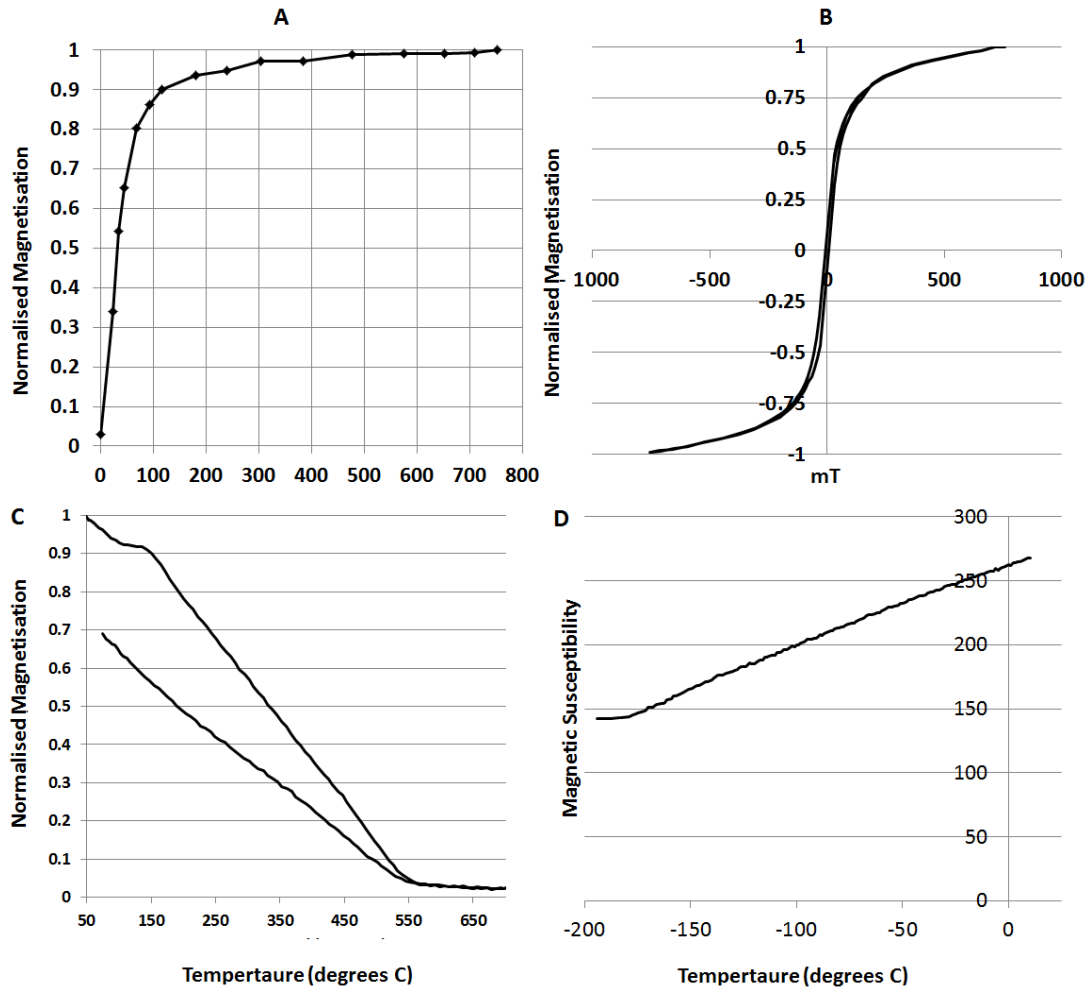


**Fig. S3.** Mineral magnetic measurements of sample PM04 from Malapa. A) IRM acquisition curve; B) Hysteresis loop; C) Thermomagnetic Curve; D) Low temperature magnetic susceptibility curve ( $10^{-5}$  SI).



**Fig. S4.** Photograph of the newly exposed flowstone layer at Malapa (A) with the locations of U-Pb samples M6 (C) and M7 (B), and new palaeomagnetic sample PM10 (D), scale bars 10cm.

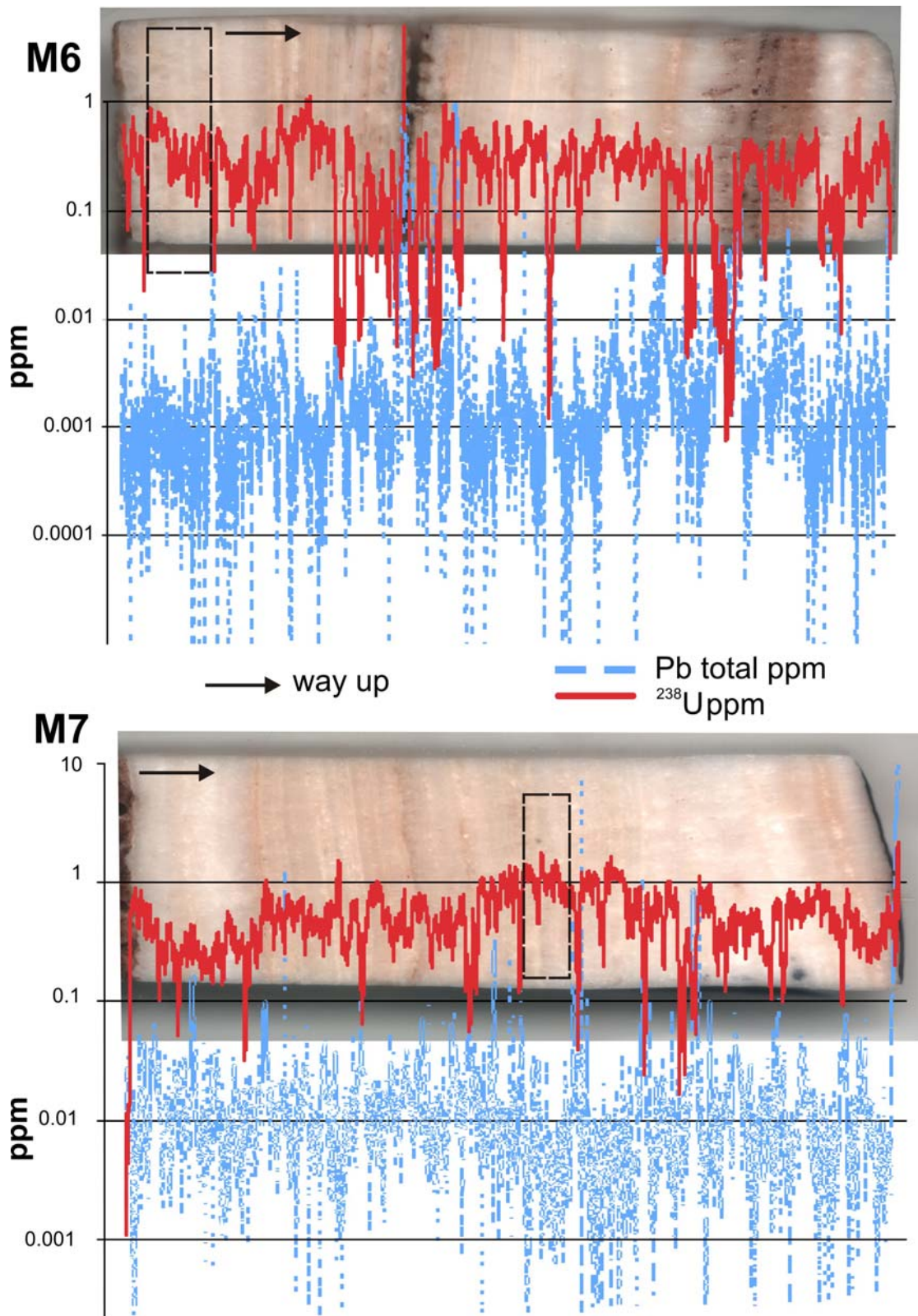


**Fig. S5.** Laser ablation U and Pb concentration profiles plotted against flowstone samples M6 and M7 with areas targeted for dating marked with a dashed box.

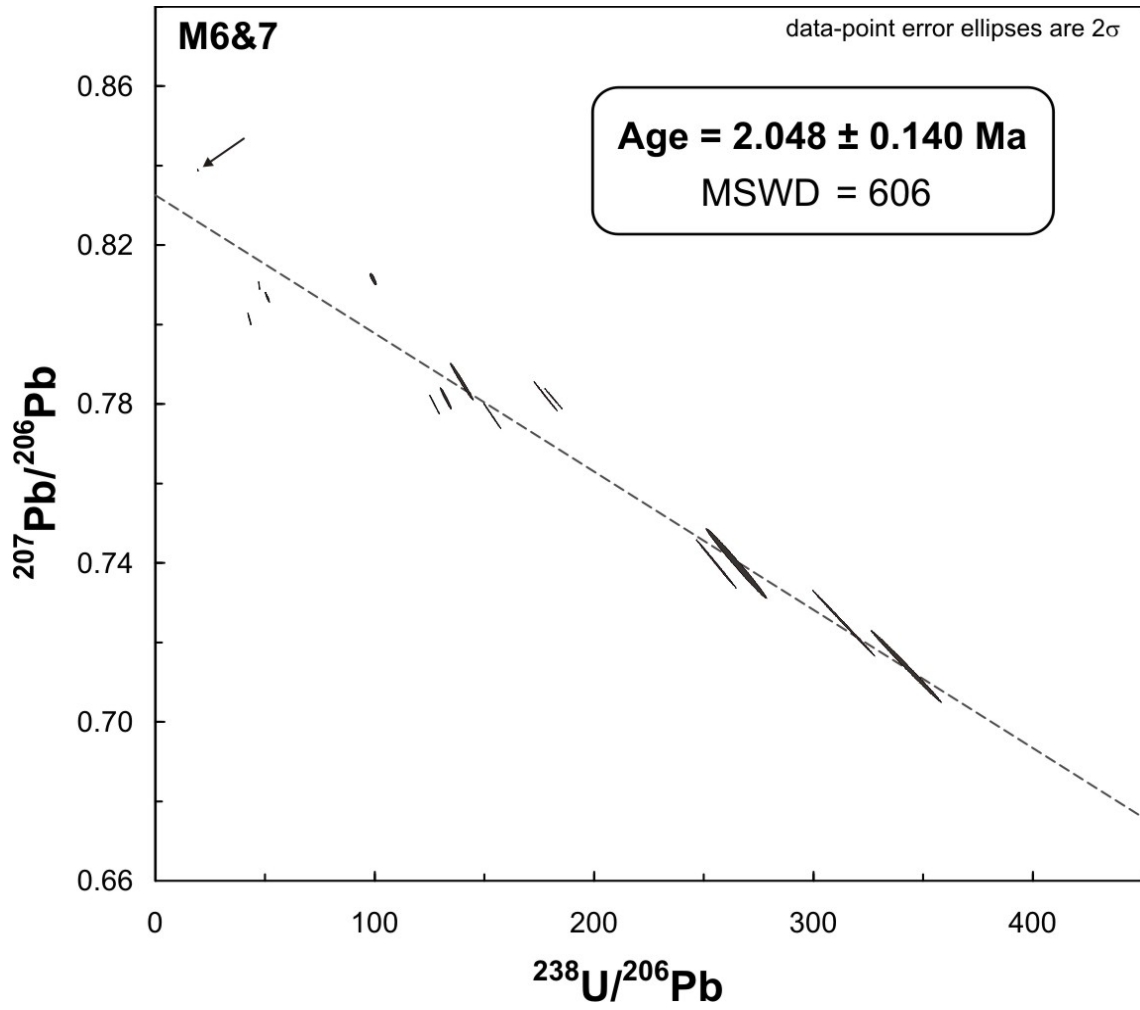


**Fig. S6.** Tera-Wasserberg age plot for Flowstone 2.

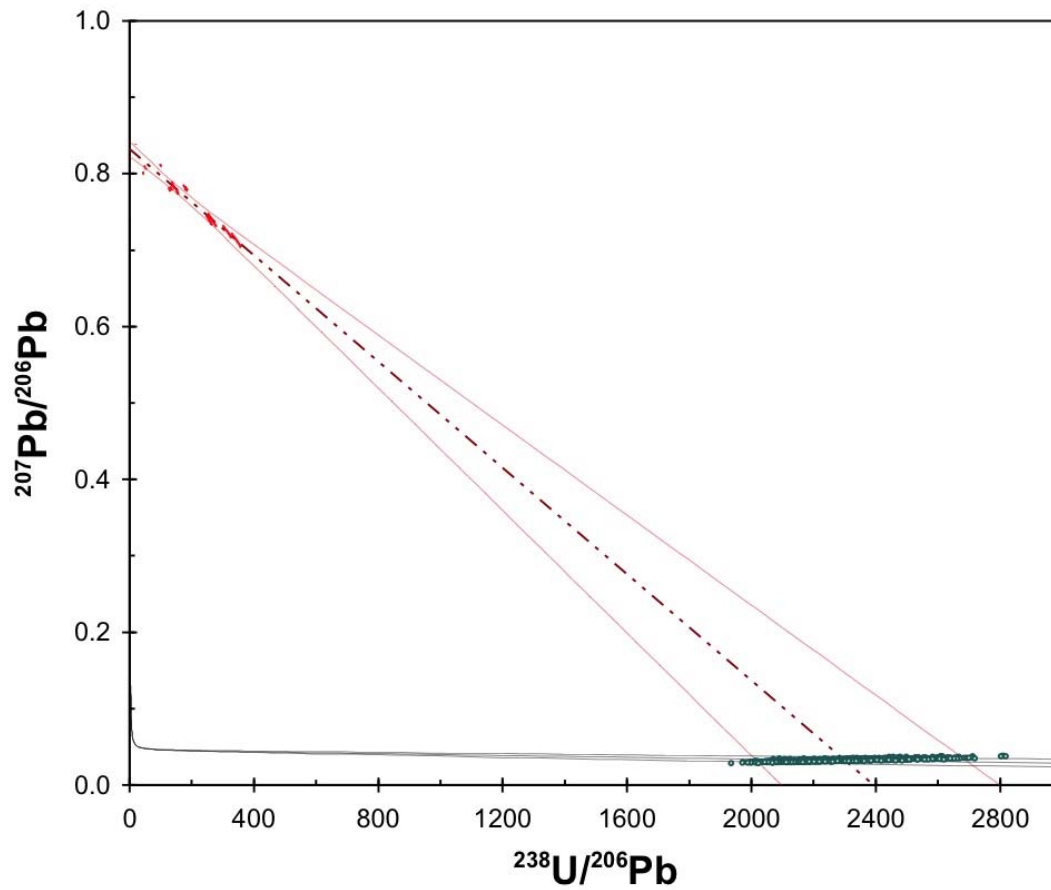


**Fig S7.** Extrapolated view of the linear fit of fig S6, showing its  $2\sigma$  uncertainty envelope and intercept with disequilibrium concordia for  $[^{234}\text{U}/^{238}\text{U}]_i$  of 2.73, 3.47 and 4.23. The green dots are a 1000-point Monte-Carlo simulation of the disequilibrium-corrected age.

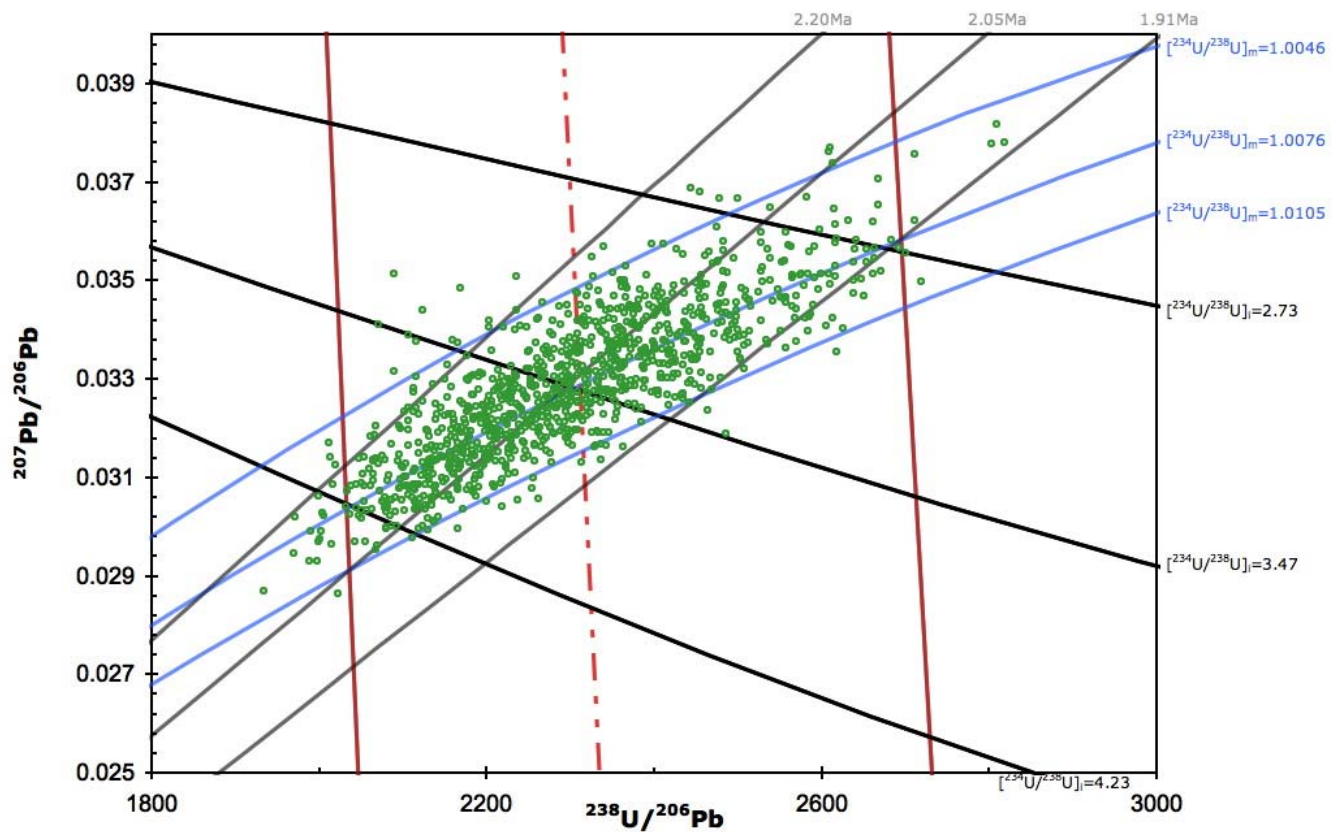


**Fig S8.** Expansion of the disequilibrium concordia (black) intercept of the linear fit to data (red) of fig S7. Measured  $[^{234}\text{U}/^{238}\text{U}]$  is in blue, and disequilibrium isochrons in grey. The disequilibrium concordia and isochrons depicted are outputs of a 1000-point Monte-Carlo simulation (green) which took the linear fit and measured  $[^{234}\text{U}/^{238}\text{U}]$  as its inputs.

## References and Notes

1. R. Pickering, J. D. Kramers, Re-appraisal of the stratigraphy and determination of new U-Pb dates for the Sterkfontein hominin site, South Africa. *J. Hum. Evol.* **59**, 70 (2010). [doi:10.1016/j.jhevol.2010.03.014](https://doi.org/10.1016/j.jhevol.2010.03.014) [Medline](#)
2. L. R. Berger *et al.*, *Australopithecus sediba*: A new species of *Homo*-like australopith from South Africa. *Science* **328**, 195 (2010). [doi:10.1126/science.1184944](https://doi.org/10.1126/science.1184944) [Medline](#)
3. P. H. Dirks *et al.*, Geological setting and age of *Australopithecus sediba* from southern Africa. *Science* **328**, 205 (2010). [doi:10.1126/science.1184950](https://doi.org/10.1126/science.1184950) [Medline](#)
4. M. Balter, From Science's Online Daily News Site. *Science* **328**, 155 (2010). [doi:10.1126/science.328.5975.155](https://doi.org/10.1126/science.328.5975.155)
5. M. Cherry, South African science: Black, white and grey. *Nature* **463**, 726 (2010). [Medline](#)
6. The *H. erectus* hypodigm includes African specimens that are referred to the taxon *H. ergaster* by some.
7. B. A. Wood, *Koobi Fora Research Project, Volume 4: Hominid Cranial Remains* (Oxford Univ. Press, Oxford, 1991).
8. R. Pickering, J. D. Kramers, P. J. Hancox, D. J. de Ruiter, J. D. Woodhead, Contemporary flowstone development links early hominin bearing cave deposits in South Africa. *Earth Planet. Sci. Lett.* **306**, 23 (2011). [doi:10.1016/j.epsl.2011.03.019](https://doi.org/10.1016/j.epsl.2011.03.019)
9. R. Ferring *et al.*, Earliest human occupations at Dmanisi (Georgian Caucasus) dated to 1.85–1.78 Ma. *Proc. Natl. Acad. Sci. U.S.A.* **108**, 10432 (2011). [doi:10.1073/pnas.1106638108](https://doi.org/10.1073/pnas.1106638108) [Medline](#)
10. T. D. White, in *Paleoclimate and Evolution with Emphasis on Human Origins*, E. S. Vrba, G. H. Denton, T. C. Partridge, L. H. Burckle, Eds. (Yale Univ. Press, New Haven, CT, 1995), pp. 369–384.
11. White (10) agreed that the first appearance date of *H. erectus* could be reliably established, although he accepted 1.75 Ma as the probable date.
12. W. H. Kimbel, in *The First Humans—Origin and Early Evolution of the Genus Homo*, F. E. Grine, J. G. Fleagle, R. E. F. Leakey, Eds. (Springer, New York, 2009), pp. 31–37.
13. W. H. Kimbel, D. C. Johanson, Y. Rak, Systematic assessment of a maxilla of *Homo* from Hadar, Ethiopia. *Am. J. Phys. Anthropol.* **103**, 235 (1997). [doi:10.1002/\(SICI\)1096-8644\(199706\)103:2<235::AID-AJPA8>3.0.CO;2-S](https://doi.org/10.1002/(SICI)1096-8644(199706)103:2<235::AID-AJPA8>3.0.CO;2-S) [Medline](#)
14. A. I. R. Herries, J. Shaw, Palaeomagnetic analysis of the Sterkfontein palaeocave deposits: Implications for the age of the hominin fossils and stone tool industries. *J. Hum. Evol.* **60**, 523 (2011). [doi:10.1016/j.jhevol.2010.09.001](https://doi.org/10.1016/j.jhevol.2010.09.001) [Medline](#)
15. A. P. Roberts, Geomagnetic excursions: Knowns and unknowns. *Geophys. Res. Lett.* **35**, L17307 (2008). [doi:10.1029/2008GL034719](https://doi.org/10.1029/2008GL034719)
16. J. Woodhead *et al.*, U-Pb geochronology of speleothems by MC-ICPMS. *Quat. Geochronol.* **1**, 208 (2006). [doi:10.1016/j.quageo.2006.08.002](https://doi.org/10.1016/j.quageo.2006.08.002)

17. R. Pickering, J. D. Kramers, T. C. P. Partridge, J. Kodolanyi, T. Pettke, U-Pb dating of calcite-aragonite layers in speleothems from hominin sites in South Africa by MC-ICP-MS. *Quat. Geochronol.* **5**, 544 (2010). [doi:10.1016/j.quageo.2009.12.004](https://doi.org/10.1016/j.quageo.2009.12.004)
18. J. E. T. Channell, A. Mazaud, P. Sullivan, S. Turner, M. E. Raymo, Geomagnetic excursions and paleointensities in the Matuyama Chron at Ocean Drilling Program Sites 983 and 984 (Iceland Basin). *J. Geophys. Res.* **107**, 2114 (2002). [doi:10.1029/2001JB000491](https://doi.org/10.1029/2001JB000491)
19. B. A. Carlson *et al.*, Brain evolution triggers increased diversification of electric fishes. *Science* **332**, 583 (2011). [doi:10.1126/science.1201524](https://doi.org/10.1126/science.1201524) [Medline](#)
20. J. M. Kibii *et al.*, *Science* **333**, 1407 (2011).
21. B. Zipfel *et al.*, *Science* **333**, 1417 (2011).
22. T. L. Kivell, *Science* **333**, 1411 (2011).
23. K. Kuman, R. J. Clarke, Stratigraphy, artefact industries and hominid associations for Sterkfontein, member 5. *J. Hum. Evol.* **38**, 827 (2000). [doi:10.1006/jhev.1999.0392](https://doi.org/10.1006/jhev.1999.0392) [Medline](#)
24. W. H. Kimbel, Y. Rak, in *Species, Species Concepts, and Primate Evolution*, W. H. Kimbel, L. B. Martin, Eds. (Plenum, New York, 1993), pp. 461–484.
25. J. C. M. Ahern, Underestimating intraspecific variation: The problem with excluding Sts 19 from *Australopithecus africanus*. *Am. J. Phys. Anthropol.* **105**, 461 (1998). [doi:10.1002/\(SICI\)1096-8644\(199804\)105:4<461::AID-AJPA5>3.0.CO;2-R](https://doi.org/10.1002/(SICI)1096-8644(199804)105:4<461::AID-AJPA5>3.0.CO;2-R) [Medline](#)
26. C. A. Lockwood, P. V. Tobias, Morphology and affinities of new hominin cranial remains from Member 4 of the Sterkfontein Formation, Gauteng Province, South Africa. *J. Hum. Evol.* **42**, 389 (2002). [doi:10.1006/jhev.2001.0532](https://doi.org/10.1006/jhev.2001.0532) [Medline](#)
27. A. R. Hughes, P. V. Tobias, A fossil skull probably of the genus *Homo* from Sterkfontein, Transvaal. *Nature* **265**, 310 (1977). [doi:10.1038/265310a0](https://doi.org/10.1038/265310a0) [Medline](#)
28. J. E. Cronin, N. T. Boaz, C. B. Stringer, Y. Rak, Tempo and mode in hominid evolution. *Nature* **292**, 113 (1981). [doi:10.1038/292113a0](https://doi.org/10.1038/292113a0) [Medline](#)
29. B. A. Wood, Who is the ‘real’ *Homo habilis*? *Nature* **327**, 187 (1987). [doi:10.1038/327187a0](https://doi.org/10.1038/327187a0) [Medline](#)
30. B. A. Wood, Origin and evolution of the genus *Homo*. *Nature* **355**, 783 (1992). [doi:10.1038/355783a0](https://doi.org/10.1038/355783a0) [Medline](#)
31. D. Curnoe, P. V. Tobias, Description, new reconstruction, comparative anatomy, and classification of the Sterkfontein Stw 53 cranium, with discussions about the taxonomy of other southern African early *Homo* remains. *J. Hum. Evol.* **50**, 36 (2006). [doi:10.1016/j.jhevol.2005.07.008](https://doi.org/10.1016/j.jhevol.2005.07.008) [Medline](#)
32. R. J. Clarke, Latest information on Sterkfontein’s *Australopithecus* skeleton and a new look at *Australopithecus*. *S. Afr. J. Sci.* **104**, 443 (2008). [doi:10.1590/S0038-23532008000600015](https://doi.org/10.1590/S0038-23532008000600015)
33. D. Curnoe, A review of early *Homo* in southern Africa focusing on cranial, mandibular and dental remains, with the description of a new species (*Homo gautengensis* sp. nov.). *Homo* **61**, 151 (2010). [doi:10.1016/j.jchb.2010.04.002](https://doi.org/10.1016/j.jchb.2010.04.002) [Medline](#)

34. J. Moggi-Cecchi, P. V. Tobias, A. D. Beynon, The mixed dentition and associated skull fragments of a juvenile fossil hominid from Sterkfontein, South Africa. *Am. J. Phys. Anthropol.* **106**, 425 (1998). [doi:10.1002/\(SICI\)1096-8644\(199808\)106:4<425::AID-AJPA2>3.0.CO;2-I](https://doi.org/10.1002/(SICI)1096-8644(199808)106:4<425::AID-AJPA2>3.0.CO;2-I) [Medline](#)
35. L. R. Berger, R. Lacruz, D. J. De Ruiter, Revised age estimates of *Australopithecus*-bearing deposits at Sterkfontein, South Africa. *Am. J. Phys. Anthropol.* **119**, 192 (2002). [doi:10.1002/ajpa.10156](https://doi.org/10.1002/ajpa.10156) [Medline](#)
36. J. Martyn, Pleistocene deposits and new fossil localities in Kenya. *Nature* **215**, 476 (1967). [doi:10.1038/215476a0](https://doi.org/10.1038/215476a0) [Medline](#)
37. A. Hill, S. Ward, A. Deino, G. Curtis, R. Drake, Earliest *Homo*. *Nature* **355**, 719 (1992). [doi:10.1038/355719a0](https://doi.org/10.1038/355719a0) [Medline](#)
38. We have not seen the excavation report cited in (36), thus it could potentially confirm the provenience of the specimen.
39. R. J. Sherwood, S. C. Ward, A. Hill, The taxonomic status of the Chemeron temporal (KNM-BC 1). *J. Hum. Evol.* **42**, 153 (2002). [doi:10.1006/jhev.2000.0409](https://doi.org/10.1006/jhev.2000.0409) [Medline](#)
40. D. Falk, E. Baker, Earliest *Homo* debate. *Nature* **358**, 289 (1992). [doi:10.1038/358289b0](https://doi.org/10.1038/358289b0) [Medline](#)
41. P. V. Tobias, Earliest *Homo* not proven. *Nature* **361**, 307 (1993). [doi:10.1038/361307a0](https://doi.org/10.1038/361307a0) [Medline](#)
42. C. A. Lockwood, W. H. Kimbel, J. Lynch, *Am. J. Phys. Anthropol.* **S34**, 102 (2002).
43. B. Asfaw *et al.*, *Australopithecus garhi*: A new species of early hominid from Ethiopia. *Science* **284**, 629 (1999). [doi:10.1126/science.284.5414.629](https://doi.org/10.1126/science.284.5414.629) [Medline](#)
44. F. Schrenk, T. G. Bromage, C. G. Betzler, U. Ring, Y. M. Juwayeyi, Oldest *Homo* and Pliocene biogeography of the Malawi Rift. *Nature* **365**, 833 (1993). [doi:10.1038/365833a0](https://doi.org/10.1038/365833a0) [Medline](#)
45. T. G. Bromage, F. Schrenk, F. W. Zonneveld, Paleoanthropology of the Malawi Rift: An early hominid mandible from the Chiwondo Beds, northern Malawi. *J. Hum. Evol.* **28**, 71 (1995). [doi:10.1006/jhev.1995.1007](https://doi.org/10.1006/jhev.1995.1007)
46. C. Betzler, U. Ring, Sedimentology of the Malawi Rift: Facies and stratigraphy of the Chiwondo Beds, northern Malawi. *J. Hum. Evol.* **28**, 23 (1995). [doi:10.1006/jhev.1995.1004](https://doi.org/10.1006/jhev.1995.1004)
47. T. G. Bromage, F. Schrenk, Y. M. Juwayeyi, Paleobiogeography of the Malawi Rift: Age and vertebrate paleontology of the Chiwondo Beds, northern Malawi. *J. Hum. Evol.* **28**, 37 (1995). [doi:10.1006/jhev.1995.1005](https://doi.org/10.1006/jhev.1995.1005)
48. O. Sandrock, O. Kullmer, F. Schrenk, Y. M. Juwayeyi, T. G. Bromage, in *Hominin Environments in the East African Pliocene*, R. Bobe, Z. Alemseged, A. K. Behrensmeyer, Eds. (Springer, Heidelberg, Germany 2007), pp. 315–332.
49. M. Beden, in *Koobi Fora Research Project, Volume 2. The Fossil Ungulates: Proboscidea, Perissodactyla and Suidae*, J. M. Harris Ed. (Clarendon Press, Oxford, 1983), pp. 40–129.

50. V. Eisenmann, in *Earliest Man and Environments in the Lake Rudolf Basin*, Y. Coppens, F. C. Howell, G. L. Isaac, R. E. F. Leakey, Eds. (Univ. of Chicago Press, Chicago, IL, 1976), pp. 225–233.
51. V. Eisenmann, in *Earliest Man and Environments in the Lake Rudolf Basin*, Y. Coppens, F. C. Howell, G. L. Isaac, R. E. F. Leakey, Eds. (Univ. of Chicago Press, Chicago, IL, 1976), pp. 234–237.
52. T. D. White, in *Paleoclimate and Evolution with Emphasis on Human Origins*, E. S. Vrba, G. H. Denton, T. C. Partridge, L. H. Burckle, Eds. (Yale Univ. Press, New Haven, CT, 1995), pp. 369–384.
53. F. C. Howell, P. Haesaerts, J. de Heinzelin, Depositional environments, archeological occurrences and hominids from Members E and F of the Shungura Formation (Omo basin, Ethiopia). *J. Hum. Evol.* **16**, 665 (1987). [doi:10.1016/0047-2484\(87\)90019-4](https://doi.org/10.1016/0047-2484(87)90019-4)
54. G. Suwa, T. D. White, F. C. Howell, Mandibular postcanine dentition from the Shungura Formation, Ethiopia: Crown morphology, taxonomic allocations, and Plio-Pleistocene hominid evolution. *Am. J. Phys. Anthropol.* **101**, 247 (1996). [doi:10.1002/\(SICI\)1096-8644\(199610\)101:2<247::AID-AJPA9>3.0.CO;2-Z](https://doi.org/10.1002/(SICI)1096-8644(199610)101:2<247::AID-AJPA9>3.0.CO;2-Z) [Medline](#)
55. S. Prat *et al.*, First occurrence of early *Homo* in the Nachukui Formation (West Turkana, Kenya) at 2.3–2.4 Myr. *J. Hum. Evol.* **49**, 230 (2005). [doi:10.1016/j.jhevol.2005.03.009](https://doi.org/10.1016/j.jhevol.2005.03.009) [Medline](#)
56. G. H. Sperber, thesis, University of the Witwatersrand, Johannesburg, South Africa (1973).
57. J. T. Robinson, *The Dentition of the Australopithecinae* (Transvaal Museum Memoir No. 9, Pretoria, South Africa, 1956).
58. W. H. Kimbel *et al.*, Late Pliocene *Homo* and Oldowan Tools from the Hadar Formation (Kada Hadar Member), Ethiopia. *J. Hum. Evol.* **31**, 549 (1996). [doi:10.1006/jhev.1996.0079](https://doi.org/10.1006/jhev.1996.0079)
59. C. J. Campisano, C. S. Feibel, *Geol. Soc. Am. Spec. Pap.* **446**, 135 (2008).
60. D. E. Lieberman, Making behavioral and phylogenetic inferences from hominid fossils: Considering the developmental influence of mechanical forces. *Annu. Rev. Anthropol.* **26**, 185 (1997). [doi:10.1146/annurev.anthro.26.1.185](https://doi.org/10.1146/annurev.anthro.26.1.185)
61. R. Dawkins, *The Greatest Show on Earth: The Evidence for Evolution* (Free Press, New York, 2009).
62. A. I. R. Herries, P. J. Hopley, J. W. Adams, D. Curnoe, M. A. Maslin, Letter to the editor: Geochronology and palaeoenvironments of Southern African hominin-bearing localities—A reply to Wrangham *et al.*, 2009. “Shallow-water habitats as sources of fallback foods for hominins”. *Am. J. Phys. Anthropol.* **143**, 640 (2010). [doi:10.1002/ajpa.21389](https://doi.org/10.1002/ajpa.21389)
63. A. G. Latham, D. C. Ford, in *Applications of Paleomagnetism to Sedimentary Geology*, D. M. Aissaoui, D. F. McNeill, N. F. Hurley, Eds. (Society of Economic Paleontologists and Mineralogists, Tulsa, OK, 1993), pp. 150–155.
64. A. I. R. Herries, J. W. Adams, K. L. Kuykendall, J. Shaw, Speleology and magnetobiostratigraphic chronology of the GD 2 locality of the Gondolin hominin-

- bearing paleocave deposits, North West Province, South Africa. *J. Hum. Evol.* **51**, 617 (2006). [doi:10.1016/j.jhevol.2006.07.007](https://doi.org/10.1016/j.jhevol.2006.07.007) [Medline](#)
65. C. Laj, J. E. T. Channell, in *Treatise on Geophysics: Geomagnetism*, M. Kono, Ed. (Elsevier, Amsterdam, 2007), 5, pp. 373–416.
66. F. Gradstein, J. Ogg, A. Smith, *A Geologic Time Scale 2004* (Cambridge Univ. Press, Cambridge, 2004).
67. M. J. Sier *et al.*, Direct terrestrial-marine correlation demonstrates surprisingly late onset of the last interglacial in central Europe. *Quat. Res.* **75**, 213 (2011). [doi:10.1016/j.yqres.2010.11.003](https://doi.org/10.1016/j.yqres.2010.11.003)
68. X. Quidelleur, J. W. Holt, T. Salvany, H. Bouquerel, New K-Ar ages from La Montagne massif, Réunion Island (Indian Ocean), supporting two geomagnetic events in the time period 2.2-2.0 Ma. *Geophys. J. Int.* **182**, 699 (2010). [doi:10.1111/j.1365-246X.2010.04651.x](https://doi.org/10.1111/j.1365-246X.2010.04651.x)
69. M. A. Lanphere, D. E. Champion, R. L. Christiansen, G. A. Izett, J. D. Obradovich, Revised ages for tuffs of the Yellowstone Plateau volcanic field: Assignment of the Huckleberry Ridge Tuff to a new geomagnetic polarity event. *Geol. Soc. Am. Bull.* **114**, 559 (2002). [doi:10.1130/0016-7606\(2002\)114<0559:RAFTOT>2.0.CO;2](https://doi.org/10.1130/0016-7606(2002)114<0559:RAFTOT>2.0.CO;2)
70. D. R. Braun *et al.*, *Proc. Natl. Acad. Sci.* **107**, 10002 (2010).
71. J. M. Cole *et al.*, Phosphor imaging as a tool for in situ mapping of ppm levels of uranium and thorium in rocks and minerals. *Chem. Geol.* **193**, 127 (2002). [doi:10.1016/S0009-2541\(02\)00223-1](https://doi.org/10.1016/S0009-2541(02)00223-1)
72. J. M. Cole, E. T. Rasbury, G. N. Hanson, I. P. Montañez, V. A. Pedone, Using U-Pb ages of Miocene tufa for correlation in a terrestrial succession, Barstow Formation, California. *Bull. Geol. Soc. Am* **117**, 276 (2005). [doi:10.1130/B25553.1](https://doi.org/10.1130/B25553.1)
73. K. Ludwig, *Berkley Geochronology Center Special Publication 1a* (Berkley Geochronology Center, Berkeley, CA, 1999).

**Acknowledgments:** We thank the South African Heritage Resources and the Nash family. Funding was received from the South African Department of Science and Technology, South African National Research Foundation, Institute for Human Evolution, University of the Witwatersrand, University of the Witwatersrand's Vice Chancellor's Discretionary Fund, National Geographic Society, Palaeontological Scientific Trust, Andrew W. Mellon Foundation, Ford Foundation, U.S. Diplomatic Mission to South Africa, French Embassy of South Africa, Oppenheimer and Ackerman families, and Sir Richard Branson. Thanks also to the University of the Witwatersrand's Schools of Geosciences and Anatomical Sciences, Bernard Price Institute for Palaeontology; Gauteng Government, Gauteng Department of Agriculture, Conservation and Environment, Cradle of Humankind Management Authority; E. Mbua, P. Kiura, and V. Iminjili at the National Museums of Kenya for access to comparative specimens; and the University of Zurich 2010 Field School. For the fossil preparation, we thank C. Dube, C. Kemp, M. Kgasi, M. Languza, J. Malaza, G. Mokoma, P. Mukanela, T. Nemvhundi, M. Ngcamphalala, S. Jirah, S. Tshabalala, and C. Yates. Others who have given significant support are B. de Klerk, W. Lawrence, C. Steininger, B. Kuhn, L. Pollarolo, J. Kretzen, D. Conforti, C.

Dlamini, H. Visser, B. Nkosi, B. Louw, L. Backwell, F. Thackeray, M. Peltier, and M. Klinkmüller. Further acknowledgements are given to Texas A&M University (The Ray A. Rothrock '77 Fellowship, the Program to Enhance Scholarly and Creative Activities, and the International Research Travel Assistance Grant of Texas A&M University), Swiss National Research Foundation (PBBEP2-126195), Australian Research Council (DP0877603), University of Melbourne (McKenzie Fellowship), Liverpool University Geomagnetism Laboratory staff, AfricaArray, James Cook University, and the BHPBilliton Geosciences staff development program.